Acta Biomaterialia xxx (2012) xxx–xxx

Contents lists available at SciVerse ScienceDirect

Acta Biomaterialia

journal homepage: www.elsevier.com/locate/actabiomat

Cyclic strain anisotropy regulates valvular interstitial cell phenotype and tissue remodeling in three-dimensional culture

Russell A. Gould, Karen Chin, Thom P. Santisakultarm, Amanda Dropkin, Jennifer M. Richards, Chris B. Schaffer, Jonathan T. Butcher *

Department of Biomedical Engineering, Cornell University, Ithaca, NY 14850, USA

ARTICLE INFO

Article history:
Received 30 September 2011
Received in revised form 20 December 2011
Accepted 5 January 2012
Available online xxxx

Keywords:
Fibroblast
Tissue engineering
Wound healing
Heart valve
Bioreactor

ABSTRACT

Many planar connective tissues exhibit complex anisotropic matrix fiber arrangements that are critical to their biomechanical function. This organized structure is created and modified by resident fibroblasts in response to mechanical forces in their environment. The directionality of applied strain fields changes dramatically during development, aging, and disease, but the specific effect of strain direction on matrix remodeling is less clear. Current mechanobiological inquiry of planar tissues is limited to equibiaxial or uniaxial stretch, which inadequately simulates many in vivo environments. In this study, we implement a novel bioreactor system to demonstrate the unique effect of controlled anisotropic strain on fibroblast behavior in three-dimensional (3-D) engineered tissue environments, using aortic valve interstitial fibroblast cells as a model system. Cell seeded 3-D collagen hydrogels were subjected to cyclic anisotropic strain profiles maintained at constant areal strain magnitude for up to 96 h at 1 Hz. Increasing anisotropy of biaxial strain resulted in increased cellular orientation and collagen fiber alignment along the principal directions of strain and cell orientation was found to precede fiber reorganization. Cellular proliferation and apoptosis were both significantly enhanced under increasing biaxial strain anisotropy ($P < 0.05$). While cyclic strain reduced both vimentin and alpha-smooth muscle actin compared to unstrained controls, vimentin and alpha-smooth muscle actin expression increased with strain anisotropy and correlated with direction ($P < 0.05$). Collectively, these results suggest that strain field anisotropy is an independent regulator of fibroblast cell phenotype, turnover, and matrix reorganization, which may inform normal and pathological remodeling in soft tissues.

1. Introduction

Planar connective tissues such as the diaphragm, pericardium, and valve leaflets perform critical biomechanical functions under cyclic mechanical loading [1,2]. These tissues have evolved complex multidirectional collagenous fiber orientations that result in anisotropic mechanical properties ideally suited to their local microenvironment. Resident tissue fibroblasts continuously repair and remodel their tissue microenvironment in response to these mechanical cues, including secreting and/or degrading extracellular matrix proteins, releasing soluble growth factors, and reorganizing cell–cell/cell–matrix adhesive interactions [3,4]. Fibroblasts transition between a quiescent synthetic phenotype, characterized by homeostatic matrix turnover, to activated contractile myofibroblasts that change the underlying matrix mechanics and/or composition depending on the remodeling state of the tissue [5]. For example, during wound closure and fibrosis/scar formation, myofibroblasts elevate expression of contractile proteins and generate traction forces that create mechanical tension to pull matrix fibers together [6]. Heart valve leaflets are exposed to arguably the most demanding mechanical environment in the body, yet interstitial fibroblasts thrive and mediate significant matrix turnover [7,8]. Mechanical microenvironmental cues therefore provide strong inductive signals regulating tissue homeostasis and remodeling, but how they mediate healthy instead of pathological tissue remodeling remains poorly understood.

Mechanistic understanding of fibroblast-mediated tissue remodeling has advanced considerably with the aid of engineered tissue models that enable testing of molecular, cellular, and tissue scale mechanisms within a well-defined, repeatable, and physiologically relevant microenvironment [9]. Fibroblasts in anchored three-dimensional (3-D) hydrogels develop mechanical tension leading to increased expression of contractile proteins, enhanced matrix synthesis, and release of growth factors such as transforming growth factor-beta (TGFβ), while fibroblasts in free-floating unstressed gels remain quiescent [10]. More recently, bioreactors have been developed to apply specific mechanical strain parameters uniformly to specimens so as to isolate the underlying signaling mechanisms [11]. For example, cyclic stretching of fibroblasts

* Corresponding author. Tel.: +1 607 255 3575; fax: +1 607 255 7330.
E-mail address: jtb47@cornell.edu (J.T. Butcher).

1742-7061/$ - see front matter © 2012 Acta Materialia Inc. Published by Elsevier Ltd. All rights reserved.
doi:10.1016/j.actbio.2012.01.006

in vitro induces cytoskeleton rearrangement [12], focal adhesion clustering [13], and downstream intracellular signaling cascades leading to cell and matrix fiber reorganization [14]. While the effects of strain magnitude and frequency have been studied for some time, the unique signaling from strain directionality is much less known. Cyclic uniaxial (one direction) stretch-induced TGFβ1, collagen III and fibronectin gene expression in cardiac fibroblasts. Equiaxial (isotropic) strain, however, induced divergent responses in extracellular matrix (ECM) mRNA levels [15]. Fibroblasts have also been shown to align perpendicular to the direction of principal strain, while no-preferred direction occurs during equiaxial strain [16]. Given that planar tissues experience multi-axial strain patterns in vivo and exhibit anisotropic biomechanical properties rather than either of the above extremes [17], it is therefore critically important to understand how biaxial strain anisotropy independently affects molecular signaling, fibroblast phenotype, and matrix remodeling behavior.

While biaxial and even triaxial stretches have been applied to tissues in cylindrical configurations, such as blood vessels [18], a similar device for planar 3-D engineered tissues has not been developed. Well-defined anisotropic biaxial strain fields have to date only been applied to planar cultures on two-dimensional (2-D) substrates [19]. Biaxial (radial and circumferential) tensile strains can be applied in two dimensions using a vacuum-pressure (Flexcell) system, but strain magnitude varies in homogeneously with distance from the center of the membrane [20]. Tan et al. also generated static heterogeneous anisotropic biaxial micro-strain patterns through multi spoke and microgroove array patterned 2-D substrates [21]. We previously showed that smooth muscle cells exposed to homogeneous equiaxial stretch in 3-D culture dedifferentiate to synthetic myofibroblasts [22]. Studies with valve fibroblasts in 3-D culture have shown heterogeneous changes in cell phenotype and matrix synthesis, but these could not be directly related to specific strain profiles [23].

The objective of this study, therefore, was to test how biaxial strain anisotropy independently controls fibroblast cell phenotype and matrix remodeling in 3-D environments. We developed and implemented a novel cyclic biaxial strain bioreactor with controllable homogeneous strain field anisotropy for engineered tissue hydrogels. We hypothesized that valvular interstitial cells (VICs) would align with respect to the principal directions of strain and rapidly remodel the underlying matrix to mirror this alignment pattern. We first determined the temporal changes in cell and matrix fiber reorganization with strain anisotropy, followed by quantification of cell proliferation, apoptosis, and fibroblast phenotype.

2. Materials and methods

2.1. Bioreactor design and optimization

Our challenge was to create a bioreactor test system that enabled fabrication and stable anchoring of 3-D hydrogels, while applying a controlled multiaxial mechanical stimulation without having to disturb the tissue. We hypothesized that if elliptically shaped 3-D hydrogels were stretched uniformly along their outer perimeters, then the internal strain field would be homogeneous but biaxial. To evaluate this, finite element simulations (FEA, ANSYS Inc.) were first conducted to optimize geometric parameters for the bioreactor system. 20,000 prismatic rectangular elements were used with large strain hyperelastic (Mooney-Rivlin, modulus = 1 MPa) material properties performed on quarter-symmetric circular sections of silicone slab and platen. Both elliptical and circular slabs and/or platens were tested, with radii between 0.5 and 2 in. Platen/cassette hole diameter ratios were varied between 0.5 and 0.9. Slab thickness was varied from 2 to 6 mm, with well depth ratios ranging from 0.5 to 0.9. Finally, well centroid within the slab was translated radially from concentric to 75% of the platen radius. Design optimization criteria were to (1) maximize the number of samples testable within one cassette well, (2) maximize the size of samples testable, (3) maximize the depth of the PDMS wells, (4) maximize the possible applied strain magnitude, and (5) minimize the stress developed in the PDMS.

To fabricate these different hydrogel 3-D geometries, we developed thick elastomeric slabs instead of commonly used thin membranes (described below), which were secured between two circular aluminum flanges of a cassette (Fig. 1A). Each cassette contained four cylindrical holes (where the slabs were exposed) positioned concentrically over Teflon lined platens. Negative molds were machined from polycarbonate such that small wells would be present within the silicone slab spanning the cassette holes above the platens (Fig. 1B). Molds were designed with ellipsoidal wells of major/minor axis ratios (hereafter X and Y respectively) of 1:1, 2:1, and 4:1. Beveled edges were machined within the ellipse to ensure uniform vertical strain fields through the well edges and to secure a compression spring (Lee spring) for anchoring hydrogels. Polydimethylsiloxane (PDMS Sylgard 184, Dow Corning) was formed at a concentration of 20:1, degassed, poured into the negative molds, and solidified at 70 °C for 12 h. Slabs were then released from the molds, mounted within the aluminum cassettes, and autoclaved before use (Fig. 1C). The stage was constrained to vertical motion using shafts with linear bearings. A rotary stepper motor (34Y, Anaheim Automation) drove vertical translation through a screw-pinion gear assembly (Fig. 1D). Limit switches were mounted on either side of the translation stage to prevent overstrain and semi-automate calibration. A cold plate (CP12, Lytron) was placed underneath the stepper motor for heat transfer. Strain magnitude and frequency waveforms were applied to the motor via a controller module and custom software (DPN10601, Anaheim Automation).

2.2. 3-D hydrogel formation

Collagen hydrogel 3-D tissue constructs were created using a procedure from one previously described [24]. Briefly, porcine aortic leaflets were harvested from a local abattoir and valvular interstitial cells were isolated immediately [25]. For these experiments, 400,000 cells/ml at P4-P6 were suspended in 3× DMEM with 10% FBS (Gibco), 2 mg/ml type I collagen (BD), and 0.1 M NaOH added to neutralize the solution. Depending on the geometry (ratio of major to minor axis) of the well, different volumes of gel were added. For the 1:1, 2:1, 4:1, and control wells, 100 μl, 125 μl, 150 μl, and 125 μl respectively of gel was inoculated into the wells containing the compression springs. Gels solidified after 60 min, after which additional culture medium was added to the reservoir. The experimental controls consisted of a mechanically stressed but non-strained gel (anchored isotropic static) and a free-floating gel (unanchored isotropic state). As in other studies [26,27], hydrogels were cultured for 24 h prior to experiments, allowing the VICs to spread and compact the matrix around the springs to create a flat 3-D tissue.

2.3. Strain field calibration

Marker fields (40 μm glass beads) were placed along the well bottom, gel surface, and at the compression spring attachment points (Fig. S1). The stage was translated to different depths, and marker positions within multiple wells were imaged and digitally recorded using ImageJ. Assuming uniform deformation within small groups of three points, the local normal and shear strain field could be described by a system of equations as previously described [22] (see Supplementary material for more details).

Please cite this article in press as: Gould RA et al. Cyclic strain anisotropy regulates valvular interstitial cell phenotype and tissue remodeling in three-dimensional culture. Acta Biomater (2012), doi:10.1016/j.actbio.2012.01.006

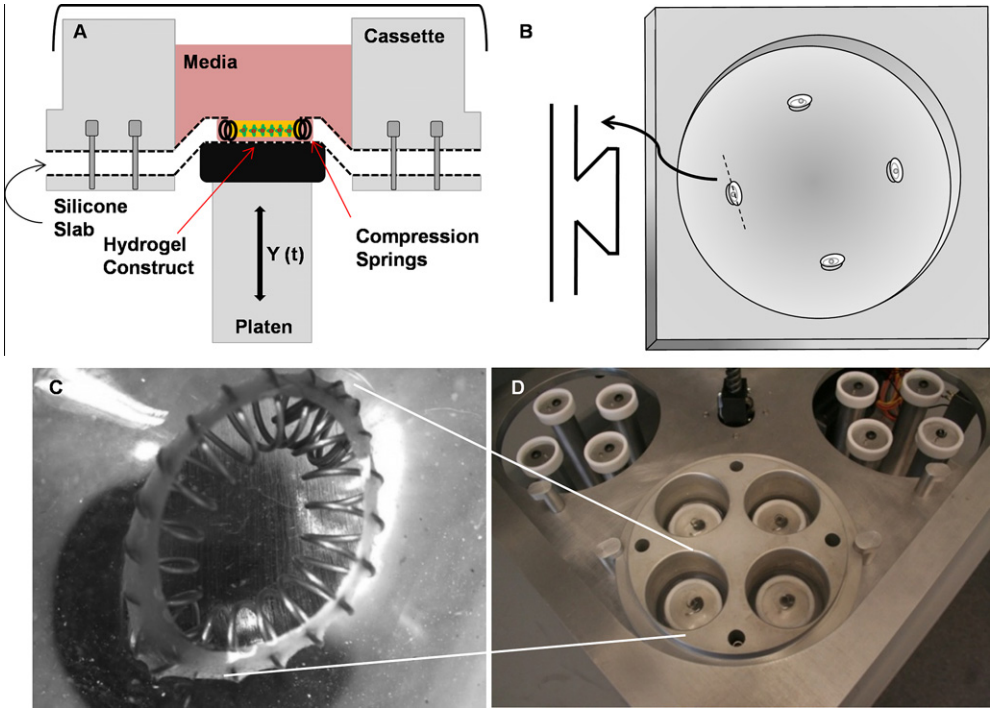

Fig. 1. Design of the anisotropic biaxial strain (ABS) bioreactor. (A) Conceptual schematic showing a cross-sectional view of a constrained collagen construct embedded in a silicone slab and loaded within an aluminum cassette. (B) An inverted polycarbonate negative mold with machined circular and elliptical wells used for constructing the silicone slab. (C) An expanded view of the elliptical well containing elliptical compression springs. (D) Macroscopic view of the bioreactor containing four cassettes and 16 independent wells.

Comparing multiple marker groups determined strain field homogeneity. At least three independent point groups were compared per well and experimental condition for calibration. For frequency response mapping, linear acceleration/deceleration-time commands of increasing magnitude and shorter time intervals were sent to the stepper motor, creating sinusoidal stage motion patterns. Peak sustainable frequencies were recorded for each applied strain magnitude (equiaxial configuration).

2.4. Biaxial strain experiments

We equalized all applied strain fields according to the apparent area strain experienced by the cells by the following formula:

$$A/A_o = \lambda_X \lambda_Y = (2E_{XX} + 1)^{0.5}(2E_{YY} + 1)^{0.5} \quad (1)$$

where A is the current area, A_o is the initial area, λ_X is the stretch ratio in the X direction, λ_Y is the stretch ratio in the Y direction, and E_{XX}/E_{YY} represent the principal strains in the XX and YY directions, respectively. We designed all biaxial strain profiles such to maintain a 20% area strain, thus only the effects of strain field anisotropy were tested. 3-D cultures with 1:1, 2:1, and 4:1 aspect ratios were stretched at 20% area strain, 1 Hz frequency for up to 96 h. Upon completion of the experiments, gels were removed from the springs and subjected to quantitative endpoint assays.

2.5. Quantification of cell and matrix architecture

We quantified changes in cell orientation and matrix fiber reorganization at 48 and 96 h via multiphoton microscopy. Image stacks of the collagen hydrogels were taken from the central region of each well at 5 μm vertical steps. Z-stacks encompassed at least 80% of the gel thickness in each sample, but were limited by the penetration depth of laser microscopy and slight differences in hydrogel compaction. Cell orientation angle distributions within each gels (0° representing the X direction) were determined using f-actin staining (Sigma) and quantified from maximum intensity projections images using ImageJ as previously described [28]. We manually traced the shape of hundreds of cells across multiple sections for each sample, and organized them within a histogram to enable comparison with the fiber alignment data. Alignment angle distributions from each gel were normalized to the most common alignment angle, which was assigned a value of 1. Simultaneously, collagen fibril alignment angle distributions were captured using second harmonic generation (SHG) imaging using a custom-built nonlinear laser scanning microscope employing 1040 nm, 1 MHz, 300 fs pulses from a Yb-fiber chirped pulse amplifier (FCPA μJewel D-400, IMRA America Inc.) as previously described [29]. Similar to the cellular orientation quantification, fiber angle distributions within gels (0° representing the X-direction) were determined using central region Z-stacks and the maximum intensity projections images processed using ImageJ. ECM fibers were analyzed in total using an alignment algorithm (adapted from Ref. [30]) that assessed second harmonic generation autofluorescence [30]. We observed no variation in histogram profiles with relative z-axis position, and therefore pooled all the data into single histograms for each construct.

2.6. Proliferation and apoptosis assays

5-Bromo-2′-deoxyuridine (BrdU) incorporation was used to detect proliferating cells. BrdU labeling reagent (Invitrogen) was added to the culture media 12 h prior to experiment termination (48 h). Hydrogel constructs were fixed and targeted with a monoclonal Anti-BrdU Alexa Fluor 488 conjugate (PRB-1, Invitrogen). Total DNA was counterstained using a DRAQ-5 (Biostatus) far red nuclear dye. TUNEL (Apo-Brdu TUNEL assay kit, Invitrogen) was used to detect apoptotic cells. 48 h stretch and control hydrogels were fixed and stained for disrupted DNA targeted by

Please cite this article in press as: Gould RA et al. Cyclic strain anisotropy regulates valvular interstitial cell phenotype and tissue remodeling in three-dimensional culture. Acta Biomater (2012), doi:10.1016/j.actbio.2012.01.006

incorporation of terminal deoxynucleotidyl transferase (Tdts) and 5-bromo-2′-deoxyuridine 5′-triphosphate (BrdUTPs). Monoclonal Ani-BrdU Alexa Fluor 488 conjugate was used to target the fragmented DNA and a propidium iodide counter stain was used to determine total cellular DNA. Positive fluorescent areas for each cell were measured using ImageJ and normalized by cell nuclei.

2.7. VIC phenotype

Alpha smooth muscle actin (gene name ACTA2, marker of myofibroblastic phenotype) and vimentin protein expression (VIM, indicative of quiescent fibroblast phenotype) were compared across strain conditions at 48 h using quantitative real-time PCR (RT-PCR, see supplemental methods) and immunohistochemistry. Antibody staining was performed as previously described [22]. Image Z-stacks (10 μm intervals) were taken with laser confocal microscopy (TCS or Leica LSM510) at fixed gain, offset, and averaging settings. Each label occupied a different fluorescence channel, and excitation lasers were sequentially activated to negate signal bleed. Z-stacks were taken at 5–10 μm sections and converted into maximum projections. Positive fluorescent areas for each color were measured using ImageJ and normalized by cell nuclei. Data was related as percentage of cells with cytoskeletal signal and compared across conditions.

2.8. Statistics

At least six samples per time point and treatment condition were used in each endpoint assay for statistical analysis. One-way ANOVA with Tukey's modified post hoc tests were used to compare differences between means and data were transformed when necessary to obtain equal sample variances. For proliferation/apoptosis studies, statistical tests were implemented across treatment conditions and results are expressed as mean ± standard error. For gene/protein expression studies, statistical tests compared individual genes across treatment conditions and results are expressed as mean ± standard deviation. $P < 0.05$ denoted statistical significance.

3. Results

3.1. Design and optimization of the anisotropic biaxial strain (ABS) bioreactor

3-D collagen gels could be anchored within cyclically deforming wells through compression springs whose lengths were adjusted to press fit inside the outer edge of the well and were secured with a 60° beveled edge (Fig. 1). Preliminary finite element simulations determined that the major and minor axis lengths of an ellipsoidal well shape could independently control *XX* and *YY* strain magnitudes (Fig. S2A). Thus, by varying the eccentricity of the elliptical well, the biaxial strain profiles scaled with the major to minor axis ratio (Fig. 2). Further simulations were done to characterize well placement within the PDMS slab and dependence upon equiaxial well diameter. Using a 1:1 geometric ratio, we found that deviations in the placement of the well, up to 60% (25 mm) along the platen radius, did not significantly affect strain magnitude (Fig. S2B). It was also determined that the strain magnitude inversely correlated with well diameter, such that a reduction of 20–10% radial strain occurred when increasing well diameter from 2 to 8 mm (Fig. S2C). Finally, parametric optimization through finite element simulations predicted that for 50 cm diameter cassette holes and 6 mm wells, a silicone slab of 3/8″ thickness with 3 mm deep wells achieved a uniform 50% strain during 1 cm of stage translation. In this configuration, four holes could be fabricated in each cassette, and four cassettes could be secured on the translating stage. For these experiments, however, one well was created at the center of each cassette hole.

We next compared our FEA simulations against measured strains of 3-D tissues within different elliptical well geometries. Stretching a 1:1 geometry introduced strains exceeding 25% ± 0.6% resulted in no significant differences between E_{XX} and E_{YY} (Fig. 2A). Conversely, a 2:1 geometry created homogeneous biaxial strain fields of at least 20% ± 1.8% in the E_{XX} and 42% ± 2.1% in the E_{YY} directions, with negligible shear strain. The applied E_{XX}/E_{YY} strain ratio was consistently 2:1 regardless of applied strain magnitude or loading cycle (Fig. 2B). Stretching 4:1 geometries introduced strains exceeding 9.1% ± 1.1% in the E_{XX} and 39% ± 1.2% in the E_{YY}, with a nearly consistent 4:1 magnitude ratio (Fig. 2C). Experimental results confirmed FEA predicted nonlinear increases in applied biaxial strain magnitudes with stage translation. For all gel ratios, shear strain E_{XY} varied between 0 ± 1.5% at the maximum loaded conditions and can be considered not statistically different from zero strain. We next determined the maximum stable strain magnitude as a function of frequency (Fig. 2D). For equiaxial profiles, a maximum strain of 27%, 18%, 12%, 8% and 5% was achieved at 1, 2, 3, 4 and 5 Hz, respectively. Peak biaxial strain magnitudes in the *YY* direction were higher at each frequency, but proportional to the area strain during equiaxial loading. Collectively, these results establish and validate a unique and versatile high-throughput anisotropic biaxial strain bioreactor system for planar 3-D tissue cultures.

3.2. Biaxial strain anisotropy regulates cellular apoptosis and proliferation

VICs seeded 3-D collagen hydrogel constructs were strained at 20% area strain, with varying biaxial anisotropies at 1 Hz, and static cultures served as controls. To verify that our bioreactor was able to maintain viable cells for at least 96 h, we performed a live/dead (green/red) assay on the hydrogel constructs. The percentage of live cells in the 1:1 (89% ± 1.3%) and 4:1 (86% ± 0.9%) geometries decreased with anisotropy compared to the percentage in anchored controls (91% ± 0.9%), but were consistently above 85% viability (Fig. 3A–E). At 48 h, the number of apoptotic cells (yellow) in the 2:1 (8.5% ± 0.3%) and 4:1 (9.6% ± 0.5%) geometries increased relative to anchored controls (5% ± 0.2%) (Fig. 3F–J). This result suggests that cell death is largely driven by strain-induced apoptosis rather than bioreactor cytotoxicity. An increase in cell proliferation was also visually apparent for the mechanically stimulated conditions at 48 h. Using BrdU labeling, we found that with increasing biaxial anisotropy, the number of proliferative cells (green) in the 1:1 (26% ± 1.9%), 2:1 (34% ± 1.4%), and 4:1 (37% ± 1.1%) geometries statistically increased relative to anchored controls (16%, ± 1%) (Fig. 3K–O). These findings suggest biaxial strain anisotropy enhances both cell proliferation and apoptosis, suggestive of an actively remodeling microenvironment.

3.3. Cell and matrix fibers rapidly reorient orthogonally with cyclic strain anisotropy

At 48 h, significantly more f-actin labeled cells were found in cyclically stretched compared to the statically anchored controls, which partly reflects both increased matrix compaction and proliferation (Fig. S3A–D). Static controls and 1:1 equiaxial strain revealed random orientations of cells denoted by the cytoskeletal (f-actin) filaments (Fig. S3E and F). Normalized cell and matrix alignment index distribution curves indicate that orientation along the major *X* (0°) and minor *Y* (90°) axes was maintained throughout a 0.3–0.8 range (Fig. S3M and N). In contrast, the 2:1 and 4:1 geometries revealed a cross-hatched network of cells aligning

Please cite this article in press as: Gould RA et al. Cyclic strain anisotropy regulates valvular interstitial cell phenotype and tissue remodeling in three-dimensional culture. Acta Biomater (2012), doi:10.1016/j.actbio.2012.01.006

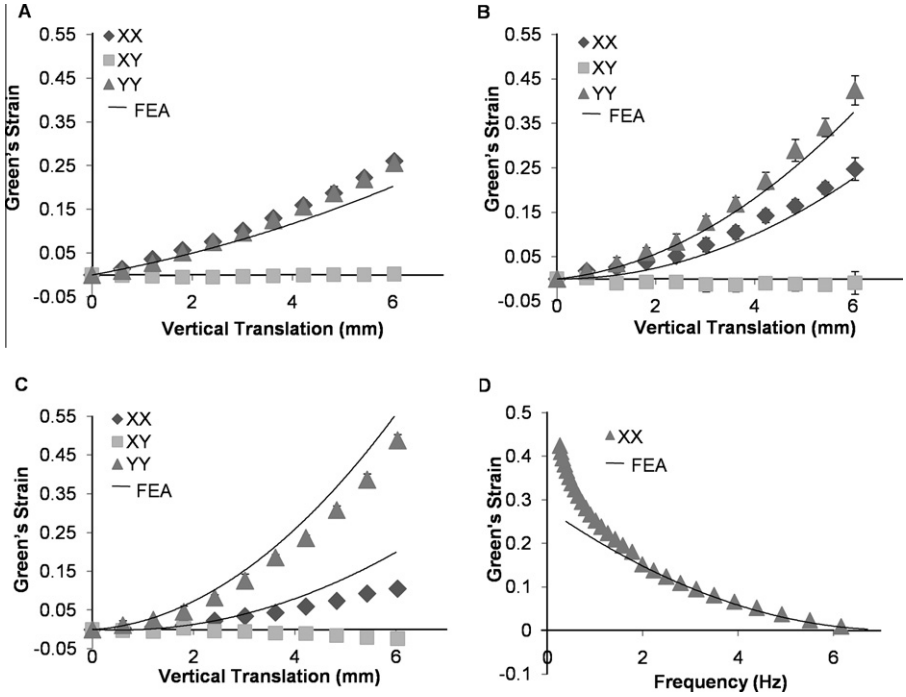

Fig. 2. Calibrated strain fields overlaid with FEA simulations. (A) 1:1 circular well introduced an equiaxial strain field with minimal shear captured by FEA simulations. (B) 2:1 ellipsoidal well introduced a biaxial strain field captured by the FEA simulations. (C) 4:1 ellipsoidal well introduced a biaxial strain field that was slightly overestimated by the FEA simulations. (D) Strain vs. frequency curves for the 1:1 geometry indicates the ability to generate large deformations at high frequencies. Error bars show ±SD. $N \geqslant 6$ samples for each geometry and strain magnitude condition.

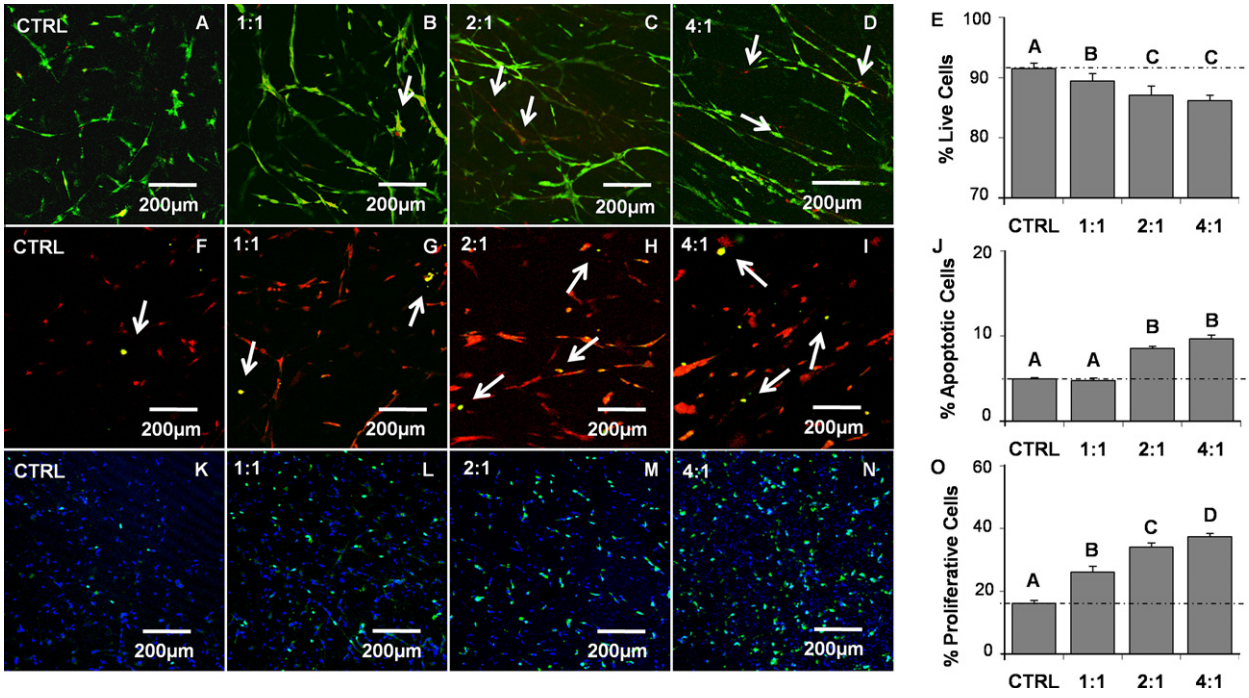

Fig. 3. Apoptosis and proliferation correlate with increasing biaxial anisotropy at 48 h. (A–D) Live/dead assay reveals an increasing amount of dead cells with increasing biaxial anisotropy (live – green, dead – red). (E) Quantification of dead cells as a percentage of total cells. (F–I) Apo-BrdU assay reveals an increasing amount of apoptotic cells with increasing biaxial anisotropy (apoptotic–yellow, DNA – red). (J) Quantification of apoptotic cells as a percentage of total cells. (K–N) BrdU labeling assay reveals an increasing amount of proliferative cells with increasing biaxial anisotropy (proliferative – green, DNA–blue). (O) Quantification of proliferative cells as a percentage of total cells. Error bars show ± SE, $N \geqslant 6$ samples per test condition. ANOVA with Tukey's post hoc testing determined statistical significance at $p \leqslant 0.05$ thresholds. Bars that do not share letters are significantly different from each other.

along the major and minor axes with greater cross-alignment in the 4:1 geometry (Fig. S3G and H). Normalized alignment curves indicate that alignment along the major and minor axes ranged from 0.90 to 0.95 and 0.50 to 0.40, respectively, while the 45°

orientation dropped to a lower fraction of 0.1–0.2 (Fig. S3O and P). Second harmonic generation imaging of collagen fibrils showed a lack of fibril alignment regardless of strained condition (Fig. S3I–L, M–P). At 96 h, static controls and 1:1 cyclic equiaxial strain revealed random orientations of cells denoted by the cytoskeletal (f-actin) filaments (Fig. 4A–B, E–F). Normalized cell and matrix alignment index distribution curves indicate that orientation along the major *X* (0°) and minor *Y* (90°) axes was maintained throughout a 0.4–0.8 range (Fig. 4M and N). In contrast, the 2:1 and 4:1 geometries revealed a cross hatched network of cells aligning along the major and minor axes with greater cross-alignment in the 4:1 geometry (Fig. 4C–D, G–H). Normalized alignment curves indicate that alignment along the major and minor axes ranged from 0.85 to 0.95 and 0.55 to 0.35, respectively, while the 45° orientation dropped to a lower fraction of 0.1–0.2 (Fig. 4O and P). Likewise, second harmonic generation imaging of collagen fibrils showed a similar trend such that increasing degrees of fibril alignment occurred with increasing anisotropic strain (Fig. 4I–L, M–P). Taken together, VICs rapidly reoriented within 48 h of cyclic strain and maintained orientation through 96 h. Extracellular matrix architecture, on the other hand, was poorly aligned at 48 h regardless of the applied strain field as determined by SHG, suggesting that cell orientation precedes fiber alignment. Collectively, these results demonstrate that applied cyclic biaxial strain anisotropy drives rapid VIC cell orientation and matrix fiber alignment in a temporally regulated manner, with cell reorientation leading extracellular matrix remodeling.

3.4. Valve interstitial cell phenotype is modulated by biaxial strain anisotropy

Alpha-smooth muscle actin (ACTA2) is a key cytoskeletal filament involved in many myofibroblastic phenotype behaviors. Within unanchored 3-D hydrogel cultures (free floating), VICs express low amounts of ACTA2. However, when cultured under anchored conditions (mechanically constrained), ACTA2 gene expression increased (2.87 ± 0.13 of control), indicating that tissue stress enhances myofibroblastic differentiation (Fig. S4). After 48 h of stretch at either the 1:1 or 2:1 geometries, ACTA2 gene expression was significantly downregulated with respect to anchored unstrained controls (expression 0.27-0.32 ± 0.05 fold of anchored control, no difference between). Stretch at the 4:1 geometry nearly doubled the amount of ACTA2 expression compared to equiaxial strain, but still less than half of the static anchored condition (0.47 ± 0.04 of control) (Fig. 5A). Vimentin (VIM) expression was insensitive to unanchored vs. anchored conditions (Fig. S4), but was significantly downregulated within the 1:1 or 2:1 geometries (0.62 ± 0.07 and 0.59 ± 0.13 respectively, no difference between). Stretch at the 4:1 geometry significantly increased VIM expression (1.13 ± 0.18 fold), recovering to control expression levels (Fig. 5A). These same trends were confirmed at the protein level via immunofluorescence (Fig. 5B–F). ACTA2 protein was downregulated significantly under equiaxial strain (0.61 ± 0.07) and slightly increased with the 4:1 geometry (0.76 ± 0.05). VIM was downregulated with equiaxial strain (0.76 ± 0.08) and then returned toward

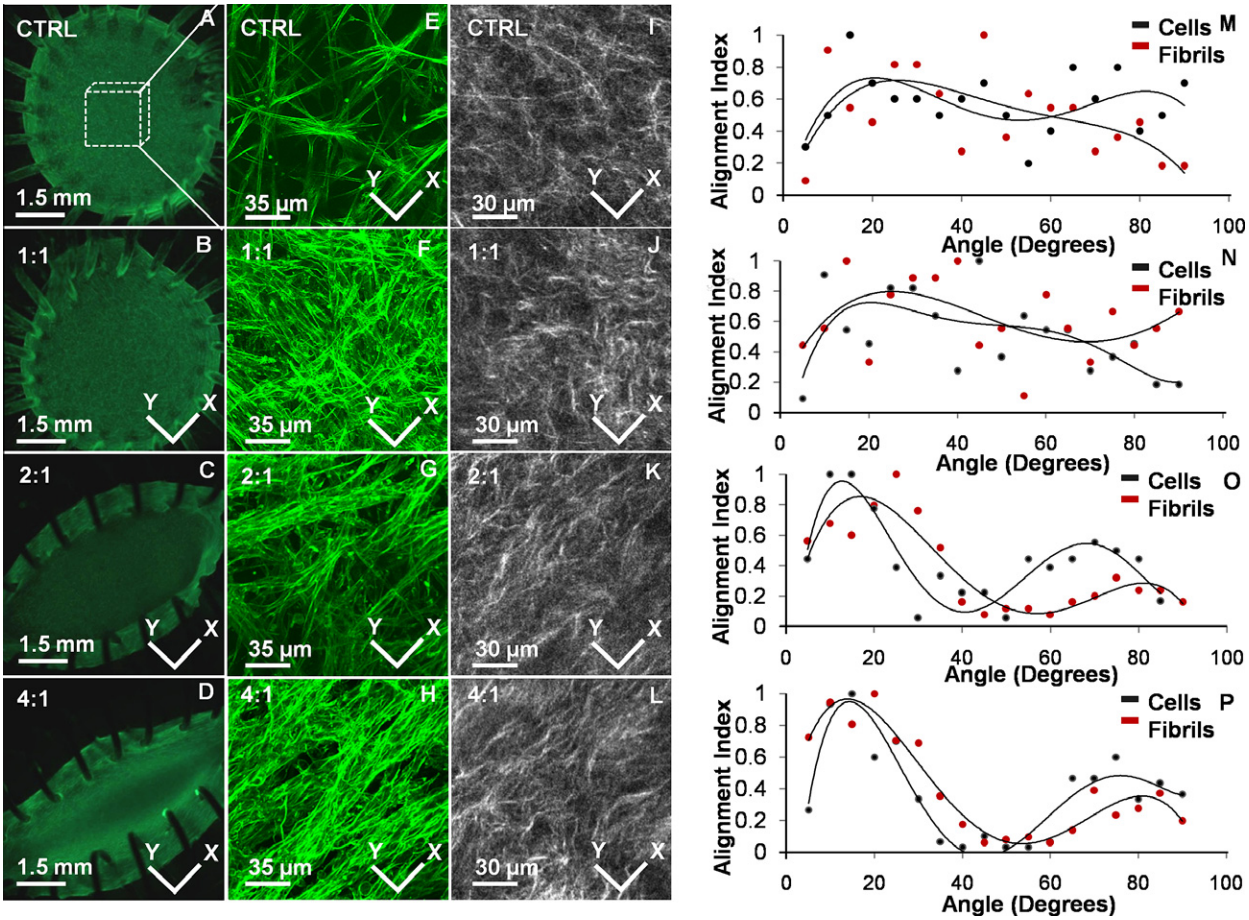

Fig. 4. Cell and matrix fibers rapidly reorient orthogonally with cyclic strain anisotropy at 96 h. (A–D) Macroscopic view of collagen gels compacted within elliptical compression springs. (E–H) Orientation of VICs associated with the anisotropic strain profiles (f-actin-green). (I–L) Orientation of collagen fibrils associated with anisotropic strain profiles (SHG imaging). (M–P) Representative alignment curves indicate orientation of both VIC and collagen fibrils coincide and align with respect to the principal directions of strain. However, a larger degree cellular orientation and fiber alignment occurs perpendicular to the first principal strain direction (*Y*).

Please cite this article in press as: Gould RA et al. Cyclic strain anisotropy regulates valvular interstitial cell phenotype and tissue remodeling in three-dimensional culture. Acta Biomater (2012), doi:10.1016/j.actbio.2012.01.006

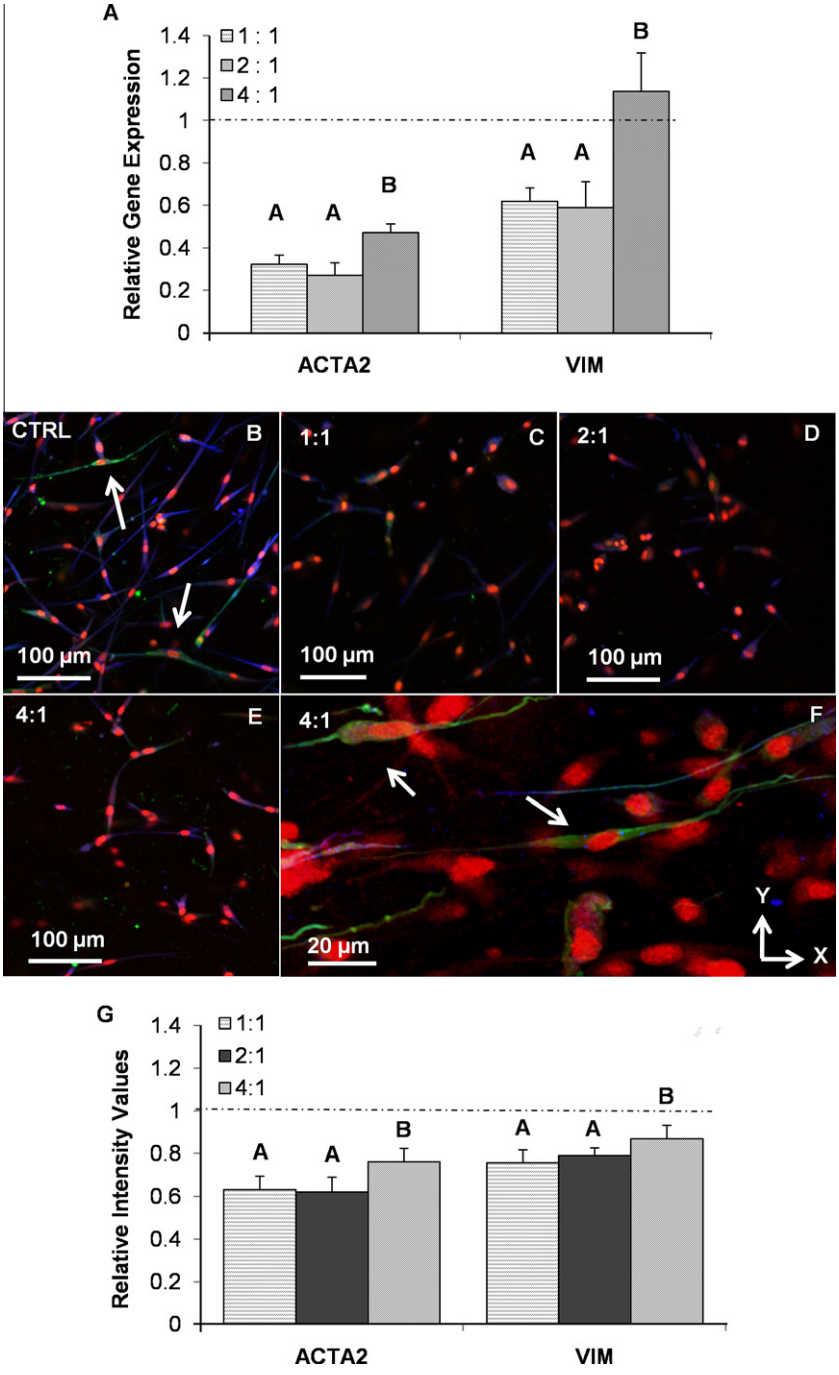

Fig. 5. Biaxial strain anisotropy modulates fibroblast cell phenotype at 48 h. (A) Gene expression was measured via real-time PCR, normalized to 18S, and expressed relative to unstretched anchored gel controls. ACTA2 gene expression decreased in all strain conditions, while VIM gene expression returned to control levels with 4:1 biaxial directionality. (B–F) ACTA2 (green) and VIM (blue) protein expression were measured via immunofluorescence with DNA (red) counterstain. (G) Quantification of total fluorescence was normalized to cell number and compared relative to unstretched control gels. (F) Although ACTA2 expression reduces with cyclic stretch, cells orienting perpendicular to the major axis of stretch expressed increased ACTA2 in the 4:1 geometry. Error bars show ± SD, $N \geqslant 6$ samples per strain geometry and protein. Bars that do not share letters are significantly different from each other as determined by one-way ANOVA with Tukey's post hoc ($p \leqslant 0.05$).

unstrained control levels with the 4:1 geometry (0.87 ± 0.06) (Fig. 5G). Interestingly, a preponderance of cells oriented parallel to the gel major axis (thus perpendicular to the greater strain direction) expressed ACTA2 protein in the 4:1 geometry (Fig. 5F). Together, this suggests that cyclic strain anisotropy independently contributes to VIC fibroblast–myofibroblast differentiation tendencies. Equibiaxial to mildly anisotropic stretch decreases ACTA2 and VIM gene and protein expression, while more dramatic strain anisotropy increases both ACTA2 and VIM expression.

4. Discussion

4.1. Anisotropic strain in vivo and in vitro

Many planar connective tissues exhibit heterogeneous matrix fiber orientations that dictate anisotropic biomechanical properties which are critical for proper function. As an example, aortic heart valve cusps are very compliant in the radial direction but stiff in the circumferential direction, which greatly assists in efficient

Please cite this article in press as: Gould RA et al. Cyclic strain anisotropy regulates valvular interstitial cell phenotype and tissue remodeling in three-dimensional culture. Acta Biomater (2012), doi:10.1016/j.actbio.2012.01.006

Coaptation and rapid opening during the cardiac cycle. Simultaneous mechanical testing and collagen fiber distribution profiling demonstrates that anisotropic fiber splay and reorientation is a key contributor to physiological valve function [31,32]. In altered loading environments, such as in hypertension or congenital malformation (e.g. bicuspid aortic valve), local cell and matrix architecture is modified with an increased risk of tissue degeneration [33–36]. Greater understanding of how strain field anisotropy controls fibroblast cell phenotype and matrix remodeling has been challenging to study in vivo due to the confounding complexity of multiple interrelated biological signals and inherent tissue variability. Applying anisotropic strains within well-controlled 3-D culture systems has been limited by (1) an inability to prescribe strain magnitudes in orthogonal directions independently, and (2) difficulties in anchoring 3-D engineered tissues within bioreactors without compromising the homogeneity and consistency (over time) of the applied strain. Pneumatic actuator based elastomeric substrate deformation is commonly applied but rate-limited by the compressibility of air, rarely exceeding 1.5 Hz for physiological soft tissue strains. Alternatively, mechanical cams require constant adjustment and repeat calibration [20,37]. Biaxial stretching of hydrogels was recently performed by molding hydrogel constructs in a cross pattern within a rotating cam [38]. However, the applied strain field was inhomogeneous and difficult to monitor over time. Furthermore, hydrogels can be adhered to elastomeric substrates via adhesive proteins, but the magnitudes of strain applicable are limited [22]. The design presented in this study overcomes these limitations by (1) prescribing strain anisotropy through eccentricity of the culture well geometry, and (2) providing uniform and stable construct attachment via compression springs. We were able to apply homogeneous large deformation strain profiles (>30%) at high frequencies (3 Hz) to engineered 3-D tissues for at least 96 h, significantly broadening the scope of 3-D in vitro mechanobiological inquiry available.

4.2. Anisotropic mechanoregulation of VIC phenotype

Fibroblasts transition between quiescent and activated myofibroblasts, which is controlled in part by the local mechanical environment. In the case of aortic valves, interstitial cells are largely quiescent fibroblasts in healthy tissue, but can become activated myofibroblasts and even osteoblasts in disease states [39–41]. Taylor et al. defines the quiescent valve fibroblast phenotype as one that maintains ECM composition and collagen maturity [42]. When VICs become activated myofibroblasts, they significantly upregulate contractile filaments including ACTA2, exhibit increased traction forces and migratory behavior, and secrete matrix proteins as well as their proteases and inhibitors. These factors all lead to dramatic changes in matrix composition and structural organization [39,42]. Grinnell et al. and colleagues have used free floating (stress-free) and anchored (stressed) collagen hydrogels to show that matrix tension induces a myofibroblastic differentiation of fibroblasts from a variety of sources [6,43,44]. We previously found that VICs cultured in 2-D flasks expressed nearly double the amount of ACTA2 when compared to seeded within floating3-D collagen gels, supporting this concept [45]. Similarly, we here find that mechanically anchored VICs in 3-D culture expressed ACTA2 nearly three times higher than unstressed controls (Fig. S4). Taken together, these results suggest that VICs in anchored 3-D collagen gels provide a simple positive-control model of myofibroblast-like differentiation.

Fibroblast–myofibroblast transitions of VICs in the context of cyclic stretch, however, are more complex. Merryman et al. showed that cyclic uniaxial stretch of porcine aortic valve leaflets for 7–14 d produced a slight increase in ACTA2 gene expression, but a marked increase with exogenous TGFβ1 administration [46]. Thayer et al. found that increased ACTA2 expression due to cyclic stretch could be relieved with combined loading with cyclic pressure [47]. Our findings here, using VICs in 3-D hydrogel culture, show that ACTA2 expression is also independently regulated by the anisotropy of applied cyclic strain. Cyclic equiaxial strain decreases ACTA2 expression, suggesting fibroblast-like tendencies, but strong directional biaxial strain re-elevates ACTA2 toward the stressed myofibroblastic control condition. We further found that ACTA2 expression was directly related to the degree of cell alignment, which occurred perpendicular to the first principal axis of stretch. Vimentin, commonly employed as a marker for fibroblasts, is an intermediate filament expressed by mesenchymal cells and responsible for cytoskeletal integrity, but not expressed exclusively by fibroblasts [48]. We found vimentin expression changed similarly with ACTA2 under cyclic stretch, but there was no change between anchored and free-floating 3-D gels, nor we did not notice a directionally dependent expression tendency like we did with ACTA2. Therefore, we are confident that vimentin was a reasonable choice as a fibroblast marker for this system, and focus our interpretations on ACTA2 and other behaviors.

Our results here demonstrate that the complete picture of fibroblast "quiescence" and "activation" should also include cell phenotype and turnover characteristics. Schnieder and Deck et al. used autoradiographic labeling in rats to demonstrate that normal cell and matrix turnovers in a variety of fibroblast-populated tissues are not identical. In fact, valve leaflets exhibited naturally elevated proliferation, matrix synthesis, and degradation rates indicative of a continuous but homeostatic remodeling environment [7]. Considering that the native healthy valve contains relatively few myofibroblasts, this suggests that phenotype "quiescence" may still present dynamic matrix remodeling behavior. Our studies here suggest that one factor that can potentiate this is mechanical forces, specifically anisotropic cyclic stretch. Cyclic biaxial strain induced both VIC proliferation and apoptosis, suggesting a high degree of turnover, while equiaxial strain exhibited significantly less. Furthermore, equiaxial strain had very little effect on matrix fiber reorganization, while cyclic anisotropic strain resulted in significantly aligned matrix fibers. Following this trend, equibiaxial stretch reduced ACTA2 expression, while anisotropic strain elevates it. Taken together, these results suggest that cyclic equiaxial strain promotes a tendency towards a quiescent fibroblastic phenotype, and increasing strain anisotropy supports a tendency towards an active myofibroblastic differentiation. We note that all these studies were performed at the same overall magnitude of area strain and frequency. While not the focus of this study, we believe that these responses are likely further altered by strain magnitude and frequency [49]. It appears that matrix remodeling lags changes in cell response to anisotropic strain, but the underlying cause is not yet known. Without live cells, however, no matrix fiber alignment occurs in any strain pattern (data not shown), suggesting that this remodeling is an active cell-mediated response to the applied strain field. Future studies considering altered matrix synthesis, degradation, or matrix fibril diameter, may help reveal the time-dependent remodeling tendencies and clarify the extent of differentiation.

4.3. Accelerated tissue engineering via strain anisotropy

Modern tissue engineering approaches for load-bearing tissues have sought to mimic or restore the native biological and biomechanical characteristics of replaced tissue, among them biomimetic material anisotropy [50]. Fiber-reinforced scaffolds, whether electrospun, nonwoven, or woven mesh designs with biodegradable materials have been employed to create directionally dependent material behaviors [51]. Alternatively, biological polymers such as collagen and fibrin can be mechanically stimulated to evolve

Please cite this article in press as: Gould RA et al. Cyclic strain anisotropy regulates valvular interstitial cell phenotype and tissue remodeling in three-dimensional culture. Acta Biomater (2012), doi:10.1016/j.actbio.2012.01.006

material heterogeneity [52,53]. Whether this anisotropy needs to be included at the outset or evolved over time is still debated. Many bioreactors designed for whole tissues expose local regions to anisotropic strain fields, but these are difficult to quantify and challenging to relate directly to local cell differentiation and matrix remodeling [54]. Alternatively, anisotropic mechanical conditioning of 3-D engineered tissue sheets could accelerate the formation of desired structural architecture and tissue biomechanics prior to forming more complex tissue shapes [55]. Furthermore, our results suggest it may be possible to direct stem/progenitor cells towards multiple distinct phenotypes through strain anisotropy, which has a potential advantage in that these cells will also be self-organized in their environmental context. It is not yet known how cells in defined 3-D matrix architectures interpret both time and directionally varying anisotropic strain fields, but our findings suggest that each component may contribute to accelerated matrix remodeling and cell differentiation.

5. Conclusions

We developed and implemented a novel bioreactor to investigate the relationship between anisotropic strain, cell differentiation, and matrix remodeling in 3-D culture. Our findings demonstrate that applied cyclic biaxial strain anisotropy induces time-dependent VIC orientation and collagen fiber alignment, which occurs at 48 h and 96 h, respectively. During this process, ACTA2 expression was directly related to the degree of cell alignment and occurred perpendicular to the principal axes of loading. These findings suggest that biaxial strain anisotropy, independent of magnitude or frequency, is a potent regulator of rapid matrix reorganization and VIC phenotype. Controlling strain anisotropy in vivo or in vitro may be a potent means of directing adaptive tissue remodeling.

Acknowledgments

We thank Glen Swan and Rodney Bowman for their design and fabrication assistance. This work was supported by The American Heart Association (#0830384N to J.T.B.), the National Science Foundation (CAREER Award CBET-0955172 to J.T.B.), the Leducq Foundation (J.T.B.), and the Hartwell Foundation (J.T.B.). The authors have no financial disclosures.

Appendix A. Figures with essential color discrimination

Certain figures in this article, particularly Figures 1, 3–5, are difficult to interpret in black and white. The full color images can be found in the on-line version, at doi:10.1016/j.actbio.2012.01.006.

Appendix B. Supplementary data

Supplementary data associated with this article can be found, in the online version, at doi:10.1016/j.actbio.2012.01.006.

References

[1] Sacks MS. Biaxial mechanical evaluation of planar biological materials. J Elast 2000;61(1–3):199–246.
[2] Sacks MS, Schoen FJ, Mayer JE. Bioengineering challenges for heart valve tissue engineering. Annu Rev Biomed Eng 2009;11:289–313.
[3] Sodian, R., et al., Early in vivo experience with tissue-engineered trileaflet heart valves. Circulation, 2000;102(19 Suppl 3):p. III22-9.
[4] Rabkin-Aikawa E et al. Clinical pulmonary autograft valves: pathologic evidence of adaptive remodeling in the aortic site. J Thorac Cardiovasc Surg 2004;128(4):552–61.
[5] Gabbiani G. The myofibroblast in wound healing and fibrocontractive diseases. J Pathol 2003;200(4):500–3.
[6] Grinnell F. Fibroblasts, myofibroblasts, and wound contraction. J Cell Biol 1994;124(4):401–4.
[7] Schneider PJ, Deck JD. Tissue and cell renewal in the natural aortic valve of rats: an autoradiographic study. Cardiovasc Res 1981;15(4):181–9.
[8] Butcher JT, Mahler GJ, Hockaday LA. Aortic valve disease and treatment: the need for naturally engineered solutions. Adv Drug Deliv Rev 2011. doi:10.1016/j.addr.2011.01.008.
[9] Bell E, Ivarsson B, Merrill C. Production of a tissue-like structure by contraction of collagen lattices by human fibroblasts of different proliferative potential in vitro. Proc Natl Acad Sci USA 1979;76(3):1274–8.
[10] Grinnell F, Ho CH. Transforming growth factor beta stimulates fibroblast-collagen matrix contraction by different mechanisms in mechanically loaded and unloaded matrices. Exp Cell Res 2002;273(2):248–55.
[11] Brown TD. Techniques for mechanical stimulation of cells in vitro: a review. J Biomech 2000;33(1):3–14.
[12] Smith PG et al. Mechanical strain increases cell stiffness through cytoskeletal filament reorganization. Am J Physiol Lung Cell Mol Physiol 2003;285(2):L456–63.
[13] Shyy JY, Chien S. Role of integrins in cellular responses to mechanical stress and adhesion. Curr Opin Cell Biol 1997;9(5):707–13.
[14] Wang JH et al. Mechanoregulation of gene expression in fibroblasts. Gene 2007;391(1–2):1–15.
[15] Lee AA et al. Differential responses of adult cardiac fibroblasts to in vitro biaxial strain patterns. J Mol Cell Cardiol 1999;31(10):1833–43.
[16] Culbertson EJ et al. Loss of mechanical strain impairs abdominal wall fibroblast proliferation, orientation, and collagen contraction function. Surgery 2011;150(3):410–7.
[17] Ogden RW. Nonlinear elasticity, anisotropy, material stability, and residual stresses in soft tissue. CISM Courses and Lectures No. 441. New York: Springer; 2003. p. 65–108.
[18] Zaucha MT et al. A novel cylindrical biaxial computer-controlled bioreactor and biomechanical testing device for vascular tissue engineering. Tissue Eng Part A 2009;15(11):3331–40.
[19] Hornberger TA et al. Intracellular signaling specificity in response to uniaxial vs. multiaxial stretch: implications for mechanotransduction. Am J Physiol Cell Physiol 2005;288(1):C185–94.
[20] Ku CH et al. Collagen synthesis by mesenchymal stem cells and aortic valve interstitial cells in response to mechanical stretch. Cardiovasc Res 2006;71(3):548–56.
[21] Tan W et al. Development and evaluation of microdevices for studying anisotropic biaxial cyclic stretch on cells. Biomed Microdev 2008;10(6):869–82.
[22] Butcher JT, Barrett BC, Nerem RM. Equibiaxial strain stimulates fibroblastic phenotype shift in smooth muscle cells in an engineered tissue model of the aortic wall. Biomaterials 2006;27(30):5252–8.
[23] Gupta V, Grande-Allen KJ. Effects of static and cyclic loading in regulating extracellular matrix synthesis by cardiovascular cells. Cardiovasc Res 2006;72(3):375–83.
[24] Mahler G, Gould R, Butcher J. Isolation and culture of avian embryonic valvular progenitor cells. J Vis Exp 2010;(44):e2159. doi:10.3791/2159.
[25] Gould RA, Butcher JT. Isolation of valvular endothelial cells. J Vis Exp 2010;(46):e2158. doi:10.3791/2158.
[26] Garvin J et al. Novel system for engineering bioartificial tendons and application of mechanical load. Tissue Eng 2003;9(5):967–79.
[27] Seliktar D, Nerem RM, Galis ZS. The role of matrix metalloproteinase-2 in the remodeling of cell-seeded vascular constructs subjected to cyclic strain. Ann Biomed Eng 2001;29(11):923–34.
[28] Butcher JT et al. Unique morphology and focal adhesion development of valvular endothelial cells in static and fluid flow environments. Arterioscler Thromb Vasc Biol 2004;24(8):1429–34.
[29] Zipfel WR, Williams RM, Webb WW. Nonlinear magic: multiphoton microscopy in the biosciences. Nat Biotechnol 2003;21(11):1369–77.
[30] Bowles RD et al. Self-assembly of aligned tissue-engineered annulus fibrosus and intervertebral disc composite via collagen gel contraction. Tissue Eng Part A 2010;16(4):1339–48.
[31] Tower TT, Neidert MR, Tranquillo RT. Fiber alignment imaging during mechanical testing of soft tissues. Ann Biomed Eng 2002;30(10):1221–33.
[32] Sacks MS, Smith DB, Hiester ED. A small angle light scattering device for planar connective tissue microstructural analysis. Ann Biomed Eng 1997;25(4):678–89.
[33] Yap CH et al. Dynamic deformation characteristics of porcine aortic valve leaflet under normal and hypertensive conditions. Am J Physiol Heart Circ Physiol 2010;298(2):H395–405.
[34] Sacks MS, David Merryman W, Schmidt DE. On the biomechanics of heart valve function. J Biomech 2009;42(12):1804–24.
[35] Weinberg EJ, Kaazempur Mofrad MR. A multiscale computational comparison of the bicuspid and tricuspid aortic valves in relation to calcific aortic stenosis. J Biomech 2008;41(16):3482–7.
[36] Robicsek F et al. The congenitally bicuspid aortic valve: how does it function? Why does it fail? Ann Thorac Surg 2004;77(1):177–85.
[37] Banes AJ et al. Culturing cells in a mechanically active environment. Am Biotechnol Lab 1990;8(7):12–22.
[38] Gupta V et al. Synthesis of glycosaminoglycans in differently loaded regions of collagen gels seeded with valvular interstitial cells. Tissue Eng 2007;13(1):41–9.
[39] Rabkin-Aikawa E et al. Dynamic and reversible changes of interstitial cell phenotype during remodeling of cardiac valves. J Heart Valve Dis 2004;13(5):841–7.

[40] Chen JH et al. Identification and characterization of aortic valve mesenchymal progenitor cells with robust osteogenic calcification potential. Am J Pathol 2009;174(3):1109–19.
[41] Liu AC, Joag VR, Gotlieb AI. The emerging role of valve interstitial cell phenotypes in regulating heart valve pathobiology. Am J Pathol 2007;171(5):1407–18.
[42] Taylor PM et al. The cardiac valve interstitial cell. Int J Biochem Cell Biol 2003;35(2):113–8.
[43] Grinnell F. Fibroblast-collagen-matrix contraction: growth-factor signalling and mechanical loading. Trends Cell Biol 2000;10(9):362–5.
[44] Grinnell F. Fibroblast biology in three-dimensional collagen matrices. Trends Cell Biol 2003;13(5):264–9.
[45] Butcher JT, Nerem RM. Porcine aortic valve interstitial cells in three-dimensional culture: comparison of phenotype with aortic smooth muscle cells. J Heart Valve Dis 2004;13(3):478–85. (discussion 485–6).
[46] Merryman WD et al. Synergistic effects of cyclic tension and transforming growth factor-beta1 on the aortic valve myofibroblast. Cardiovasc Pathol 2007;16(5):268–76.
[47] Thayer P et al. The effects of combined cyclic stretch and pressure on the aortic valve interstitial cell phenotype. Ann Biomed Eng 2011;39(6):1654–67.
[48] Goldman RD et al. The function of intermediate filaments in cell shape and cytoskeletal integrity. J Cell Biol 1996;134(4):971–83.
[49] Arnoczky SP et al. Activation of stress-activated protein kinases (SAPK) in tendon cells following cyclic strain: the effects of strain frequency, strain magnitude, and cytosolic calcium. J Orthop Res 2002;20(5):947–52.
[50] Mendelson K, Schoen FJ. Heart valve tissue engineering: concepts, approaches, progress, and challenges. Ann Biomed Eng 2006;34(12):1799–819.
[51] Courtney T et al. Design and analysis of tissue engineering scaffolds that mimic soft tissue mechanical anisotropy. Biomaterials 2006;27(19):3631–8.
[52] Mol A et al. Fibrin as a cell carrier in cardiovascular tissue engineering applications. Biomaterials 2005;26(16):3113–21.
[53] Neidert MR, Tranquillo RT. Tissue-engineered valves with commissural alignment. Tissue Eng 2006;12(4):891–903.
[54] Vesely I. Heart valve tissue engineering. Circ Res 2005;97(8):743–55.
[55] L'Heureux N et al. A completely biological tissue-engineered human blood vessel. FASEB J 1998;12(1):47–56.

Please cite this article in press as: Gould RA et al. Cyclic strain anisotropy regulates valvular interstitial cell phenotype and tissue remodeling in three-dimensional culture. Acta Biomater (2012), doi:10.1016/j.actbio.2012.01.006